Photoluminescence characterization in silicon nanowire fabricated by thermal oxidation of nano-scale Si fin structure

Yoko Sakurai,[1,*] Kuniyuki Kakushima,[2] Kenji Ohmori,[1] Keisaku Yamada,[1] Hiroshi Iwai,[2] Kenji Shiraishi,[1] and Shintaro Nomura[1]

[1]*Graduate School of Pure and Applied Sciences, University of Tsukuba, Tsukuba, Japan*
[2]*Frontier Research Center, Tokyo Institute of Technology, Yokohama, Japan*
[*]*s0930093@u.tsukuba.ac.jp*

Abstract: Low-temperature photoluminescence (PL) spectra of electron-hole systems in Si nanowires (NWs) prepared by thermal oxidization of Si fin structures were studied. Mapping of PL reveals that NWs with uniform width are formed over a large area. Annealing temperature dependence of PL peak intensities was maximized at 400 °C for each NW type, which are consistent with previous reports. Our results confirmed that the micro-PL demonstrated here is one of the important methods for characterizations of the interface defects in Si NWs.

OCIS codes: (300.0300) Spectroscopy; (300.2140) Emission.

References and links

1. H. Iwai, "Roadmap for 22 nm and beyond," Microelectron. Eng. **86**(7–9), 1520–1528 (2009).
2. S. Sato, K. Kakushima, P. Ahmet, K. Ohmori, K. Natori, K. Yamada, and H. Iwai, "Structural advantages of rectangular-like channel cross-section on electrical characteristics of silicon nanowire field-effect transistors," Microelectron. Reliab. **51**(5), 879–884 (2011).
3. M. T. Björk, J. Knoch, H. Schmid, H. Riel, and W. Riess, "Silicon nanowire tunneling field-effect transistors," Appl. Phys. Lett. **92**(19), 193504 (2008).
4. J. Knoch, S. Mantl, and J. Appenzeller, "Impact of the dimensionality on the performance of tunneling FETs: Bulk versus one-dimensional devices," Solid State Electron. **51**(4), 572–578 (2007).
5. Y. Cui, Z. Zhong, D. Wang, W. U. Wang, and C. M. Lieber, "High performance silicon nanowire field effect transistors," Nano Lett. **3**(2), 149–152 (2003).
6. Y. Lee, K. Kakushima, K. Shiraishi, K. Natori, and H. Iwai, "Size-dependent properties of ballistic silicon nanowire field effect transistors," J. Appl. Phys. **107**(11), 113705 (2010).
7. Y. Cui, Q. Wei, H. Park, and C. M. Lieber, "Nanowire nanosensors for highly sensitive and selective detection of biological and chemical species," Science **293**(5533), 1289–1292 (2001).
8. A. Gao, N. Lu, Y. Wang, P. Dai, T. Li, X. Gao, Y. Wang, and C. Fan, "Enhanced sensing of nucleic acids with silicon nanowire field effect transistor biosensors," Nano Lett. **12**(10), 5262–5268 (2012).
9. B. Tian, X. Zheng, T. J. Kempa, Y. Fang, N. Yu, G. Yu, J. Huang, and C. M. Lieber, "Coaxial silicon nanowires as solar cells and nanoelectronic power sources," Nature **449**(7164), 885–889 (2007).
10. L. Tsakalakos, J. Balch, J. Fronheiser, B. A. Korevaar, O. Sulima, and J. Rand, "Silicon nanowire solar cells," Appl. Phys. Lett. **91**(23), 233117 (2007).
11. O. Hayden, A. B. Greytak, and D. C. Bell, "Core-shell nanowire light-emitting diodes," Adv. Mater. **17**(6), 701–704 (2005).
12. Y. Arakawa and H. Sakaki, "Multidimensional quantum well laser and temperature dependence of its threshold current," Appl. Phys. Lett. **40**(11), 939–941 (1982).
13. M. V. Fischetti and S. E. Laux, "Monte Carlo analysis of electron transport in small semiconductor devices including band-structure and space-charge effects," Phys. Rev. B Condens. Matter **38**(14), 9721–9745 (1988).
14. T. Ogawa and T. Takagahara, "Interband absorption spectra and Sommerfeld factors of a one-dimensional electron-hole system," Phys. Rev. B Condens. Matter **43**(17), 14325–14328 (1991).
15. T. Ogawa and T. Takagahara, "Optical absorption and Sommerfeld factors of one-dimensional semiconductors: An exact treatment of excitonic effects," Phys. Rev. B Condens. Matter **44**(15), 8138–8156 (1991).
16. P. J. Dean, J. R. Haynes, and W. F. Flood, "New radiative recombination processes involving neutral donors and acceptors in silicon and germanium," Phys. Rev. **161**(3), 711–729 (1967).
17. W. P. Dumke, "Two-phonon indirect transitions and lattice scattering in Si," Phys. Rev. **118**(4), 938–939 (1960).
18. L. V. Keldysh, "The electron-hole liquid in semiconductors," Contemp. Phys. **27**(5), 395–428 (1986).
19. W. F. Brinkman and T. M. Rice, "Electron-hole liquids in semiconductors," Phys. Rev. B **7**(4), 1508–1523 (1973).

#202699 - $15.00 USD Received 6 Dec 2013; accepted 24 Dec 2013; published 23 Jan 2014

20. J. C. Hensel, T. G. Phillips, T. M. Rice, and G. A. Thomas, *Solid States of Physics* (Academic, 1977), Vol. 32.
21. O. Demichel, F. Oehler, P. Noe, V. Calvo, N. Pauc, P. Gentile, T. Baron, D. Peyrade, and N. Magnea, "Photoluminescence of confined electron-hole plasma in core-shell silicon/silicon oxide nanowires," Appl. Phys. Lett. **93**(21), 213104 (2008).
22. D. J. Lockwood, G. C. Aers, L. B. Allard, B. Bryskiewicz, S. Charbonneau, D. C. Houghton, J. P. McCaffrey, and A. Wang, "Optical properties of porous silicon," Can. J. Phys. **70**(10-11), 1184–1193 (1992).
23. D. J. Lockwood, Z. H. Lu, and J. M. Baribeau, "Quantum confined luminescence in Si/SiO_2 superlattices," Phys. Rev. Lett. **76**(3), 539–541 (1996).
24. H. D. Barber, "Effective mass and intrinsic concentration in silicon," Solid State Electron. **10**(11), 1039–1051 (1967).
25. M. Uematsu, H. Kageshima, K. Shiraishi, M. Nagase, S. Horiguchi, and Y. Takahashi, "Two-dimensional simulation of pattern-dependent oxidation of silicon nanostructures on silicon-on-insulator substrates," Solid State Electron. **48**(6), 1073–1078 (2004).
26. H. Ohta, T. Watanabe, and I. Ohdomari, "Strain distribution around SiO_2/Si interface in Si nanowires: A Molecular dynamics Study," Jpn. J. Appl. Phys. **46**(5B), 3277–3282 (2007).
27. K. Shiraishi, M. Nagase, S. Horiguchi, H. Kageshima, M. Uematsu, Y. Takahashi, and K. Murase, "Designing of silicon effective quantum dots by using the oxidation-induced strain: a theoretical approach," Physica E **7**(3–4), 337–341 (2000).
28. S. Horiguchi, M. Nagase, K. Shiraishi, H. Kageshima, Y. Takahashi, and K. Murase, "Mechanism of potential profile formation in Silicon single-electron transistors fabricated using pattern-dependence oxidation," Jpn. J. Appl. Phys. **40**(1A–B), L29–L32 (2001).
29. Z. Liu, K. Ando, Y. Kawashima, and S. Fujieda, "Influence of H_2-annealing on the hydrogen distribution near SiO_2 / Si (100) interfaces revealed by in situ nuclear reaction analysis," J. Appl. Phys. **92**(8), 4320–4329 (2002).
30. L. D. Thanh and P. Balk, "Elimination and generation of Si/ SiO_2 interface traps by low temperature hydrogen annealing," J. Electrochem. Soc. **135**(7), 1797–1801 (1988).
31. M. L. Reed and J. D. Plummer, "Chemistry of Si-SiO_2 interface trap annealing," J. Appl. Phys. **63**(12), 5776–5793 (1988).

1. Introduction

Si nanowire (NW) field effect transistors (FETs) are one of the most promising devices for next-generation CMOS nanodevices with high speed and low operation power [1–6]. The characteristic feature of NWs that suppresses the short-channel-effect is expected to overcome the down-scaling limitation due to a huge off-state leakage current and to provide a steep inverse threshold. Moreover, achieving high-density integration of NWs enables the use of less available silicon surface per device [1]. Si NW FETs are also used to fabricate sensors for biological and chemical species [7,8]. The sensing mechanism is understood in terms of the change in the charge density at the surface of Si NW FET. Large surface/volume ratio of NW contributes to enhance the sensitivity. Another promising application of Si NWs is solar cells [9,10] expected to serve as integrated power sources for nanoelectronic systems. For optical interconnection, Si NW-based light-emitting diodes (LEDs) have attracted attentions for fabricating nanometer-scale light sources [11].

High performance of these devices is provided by the geometrical factors and physical properties inherent in confinement of carriers [12–15]. In quantum confined structures, the degrees of freedom in free-electron motion are reduced, leading to a change in the electron density of states. A peculiar feature of an ideal one-dimensional system is the inverse-square-root divergence of the joint density of states at the band-gap. In a quasi-one dimensional system with a finite NW cross-section, the cross-sectional shape of the quasi-one dimensional structure plays a critical role for its physical properties. These characteristic features of one dimensional system lead to peculiar optical properties such as an increase in the exciton binding energy, a strong concentration of the oscillator strength to the lowest exciton state [14,15] and higher gain for quantum wire lasers [13].

The interface properties between a Si NW and the surrounding SiO_2 layer are known to affect the electrical conduction of Si NWFETs. The saturation current of a Si NW is limited by, for example, the roughness of the interface, impurity levels, channel surface orientation and the cross-sectional shapes of the channel [2]. Photoluminescence (PL) and optical absorption of Si NWs are sensitive to the impurity levels, interface defect density, and the band structure of the electron and the hole originating from NW width and cross-sectional shapes of NWs. Hence, the microscopic spectroscopy is an important method for local

#202699 - $15.00 USD Received 6 Dec 2013; accepted 24 Dec 2013; published 23 Jan 2014

characterization of the interface properties of NWs, and in particular, may also be applied to characterize local properties of NW samples without electric conductance.

In this paper, we report on the results of the PL measurements of Si NWs. We investigate how PL characteristics depend on the interface properties and the spatial distribution of the properties of NWs, and show that optical measurements are useful for device characterization.

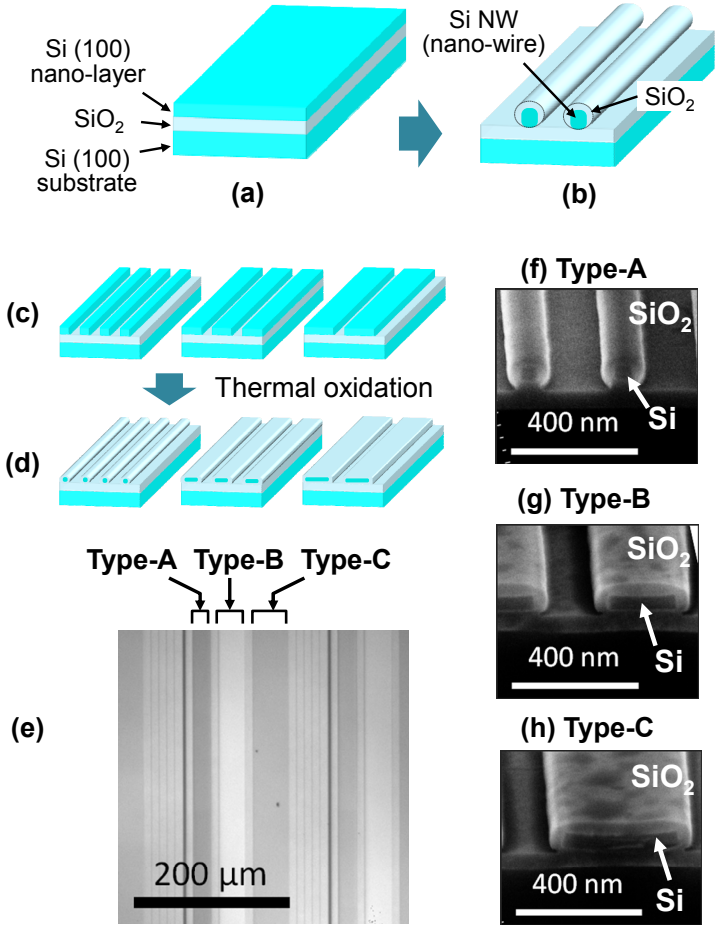

Fig. 1. (a) Schematic SOI structure used in the experiment. (b) Schematic illustration of intended Si NW structures surrounded by the thermal oxide SiO_2 layer. (c) Si NW structures with gap/width ratio of 1:1 (Type-A), 1:2 (Type-B) and 1:3 (Type-C). One hundred NWs with varied widths are patterned in each type. (d) Si NW structures finished by thermal oxidation from the state (c). (e) Top-view optical microscope photograph of the resultant Si NW sets of Type-A, -B and -C, as shown by the arrows. (f), (g) and (h) SEM images of Si NWs corresponding to Type-A, Type-B and Type-C, respectively. Si widths in each-type of 150, 300 and 450 nm before thermal oxidation were reduced to 50, 219 and 386 nm after oxidation, respectively.

2. Sample preparation

We used a (100)-oriented silicon-on-insulator (SOI) wafer with a silicon layer thickness of 70 nm obtained from SOITEC Company. Figure 1(a) shows a schematic SOI structure, while Fig. 1(b) shows a schematic diagram of the Si NW surrounded by the thermal oxide SiO_2 layer. Si NWs were prepared by the following two steps; the first step for Si fin structures fabricated by photolithography followed by reactive ion etching, as shown schematically in Fig. 1(c), and the second step for thermal oxidation of the Si fins to form the Si NWs, as

#202699 - $15.00 USD Received 6 Dec 2013; accepted 24 Dec 2013; published 23 Jan 2014

shown schematically in Fig. 1(d). Before thermal oxidation, three types of Si fin structures were patterned, that is, the structures with the gap-and-NW width ratios of 1:1 (hereinafter referred to simply as Type-A), 1:2 (Type-B), and 1:3 (Type-C). Each type has one hundred NWs with the varying Si NW widths. Table 1 shows summarized sets of structures. At the lower columns, widths before and after thermal oxidation were shown by the figures out of and within the parentheses. After thermal oxidation, Si NWs were annealed in forming gas mixed with 3% hydrogen (H_2) and 97% nitrogen (N_2) at different temperatures between 325 and 500 ^{o}C.

Figure 1(e) shows a top-view optical microscope photograph indicating layout of the resultant Si NW sets including Type-A, -B and -C, as shown by the arrows. On the other hand, scanning electron microscopic (SEM) images of Si-NW cross-sections corresponding to Type-A, Type-B and Type-C, are shown in Figs. 1(f)–1(h), respectively. The cross-section of the Type-A Si NW is nearly square, while others are flat rectangular. From these photographs, it is found that widths of Si NWs shown by rectangles in black are reduced to 50, 219 and 386 nm after thermal oxidation from initial 150, 300 and 450 nm before thermal oxidation, respectively. It is also found that the thickness of the SiO_2 layer surrounding the Si NW is about 50 nm.

Table 1. Summarized sets of Si NW structures categorized into Type-A, Type-B and Type-C depending on the NW gap/width ratio. At the lower columns, widths before and after thermal oxidation were shown by the figures out of and within the parentheses

	Type-A	Type-B	Type-C
G: W	1: 1 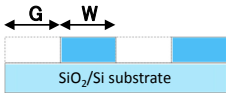	1: 2 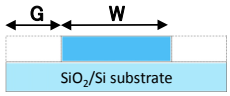	1: 3 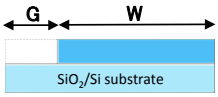
	150 nm (50 ± 5 nm)	300 nm (219 ± 5 nm)	450 nm (386 ± 5 nm)
	140 nm (37 ± 5 nm)	280 nm (203 ± 5 nm)	420 nm (347 ± 5 nm)
	130 nm (32 ± 5 nm)	260 nm (177 ± 5 nm)	390 nm (314 ± 5 nm)
	120 nm (24 ± 5 nm)	240 nm (137 ± 5 nm)	360 nm (284 ± 5 nm)

3. Photoluminescence measurement

Si NWs were characterized by a micro-PL setup, as shown schematically in Fig. 2(a). Samples were placed in a helium gas-flow cryostat at 12 K. A continuous wave He-Cd laser light at the wavelength of 325 nm was introduced to a collimator lens using a multimode optical fiber with a core diameter of 100 μm and was focused on the sample surface via a beam splitter and × 10 objective lens at an N.A. of 0.25. An incidence laser power was set to be about 280 Wcm^{-2} with a spot diameter of 31 μm on the sample surface. The PL light was collimated by the same objective lens and collected to a 0.5 m focal-length monochromator via the beam splitter, mirror and multimode optical fiber with a core diameter of 100 μm.

#202699 - $15.00 USD Received 6 Dec 2013; accepted 24 Dec 2013; published 23 Jan 2014

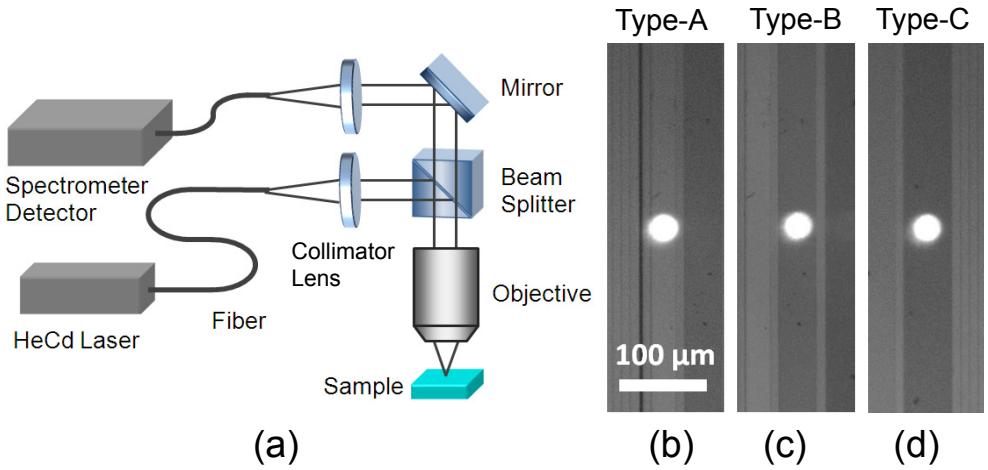

Fig. 2. (a) Schematic illustration of micro-PL setup. A continuous wave laser light at the wavelength of 325 nm was focused on the surface of the samples in a helium gas-flow cryostat at 12 K. The incidence laser power was about 280 Wcm^{-2} at the spot diameter of 31 μm on the sample surface. (b), (c) and (d) Optical microscope images of excitation spot on NWs at the Type-A, Type-B and Type-C, respectively.

Finally, it was detected by a liquid-nitrogen cooled InGaAs multichannel detector. Optical microscope images of excitation spots on the Si NWs for Type-A, Type-B and Type-C are shown by white circles in Figs. 2(b)–2(d), respectively. Here, the designed gap widths (G) / Si fin widths (W) were (b) 145 nm / 145 nm, (c) 145 nm / 290 nm and (d) 145 nm / 420 nm.

In the PL measurement, average PL emission intensity from several tens of NWs was detected with the excitation spot which covers several tens of NWs. Although the excitation spot size was set to 31 μm on the sample surface, as mentioned above, the diameter of the detection spot was set to be smaller value of 24 μm so that the uniformity of the optical excitation density of the NWs was ensured. As a reference sample, a 2 × 2 mm^2 bulk Si was placed beside the 5 × 2 mm^2 NW sample for measurement of the PL from the bulk Si. The PL intensity of the Si NWs was normalized by the PL intensity from the bulk Si in order to avoid the possible run-to-run variation in the PL measurement due to fluctuation in alignment of the optical setup and so on.

Finally, the excitation position was scanned with a PC-controlled stepping motor. The scan direction was set to be both parallel and perpendicular to the axis of the NWs by software.

4. Results and discussions

4.1 PL spectra from the Si NW chip

Figures 3(a)–3(c) show PL spectra obtained at 12 K from Si NWs with the Si width of 50 nm in Type-A, 219 nm in Type-B and 386 nm in Type-C after thermal oxidation, respectively, while Fig. 3(d) shows a PL spectrum observed from a bulk Si substrate located beside the Si NW on the same sample. In Fig. 3(d), the narrow and sharp peak at 1.098 eV is considered to originate from transverse optical (TO)-phonon assisted recombination of free excitons, while small peaks at 1.137, 1.035 and 1.075 eV are originating from transverse acoustic (TA) phonon-, TO/O^{Γ} phonon- and TO/IV^{a}-phonon assisted recombination of free excitons, respectively [16, 17]. For the case of Si NWs in Figs. 3(a)–3(c), on the other hand, such an exciton-related narrow peak at 1.098 eV appears only in Fig. 3(a), probably originating from the Si substrate at the gap between the NWs, and is not observed in Figs. 3(b) and 3(c). As shown schematically in Fig. 3(e), this is probably because coverage of the Si NW is larger, or in other words, an exposed Si substrate is smaller, in Figs. 3(b) and 3(c) (in Type-C, for

#202699 - $15.00 USD Received 6 Dec 2013; accepted 24 Dec 2013; published 23 Jan 2014

example, a ratio of NW/ Si substrate is 386nm/150nm) than in Fig. 3(a) (in Type-A, the ratio is 50nm/150nm).

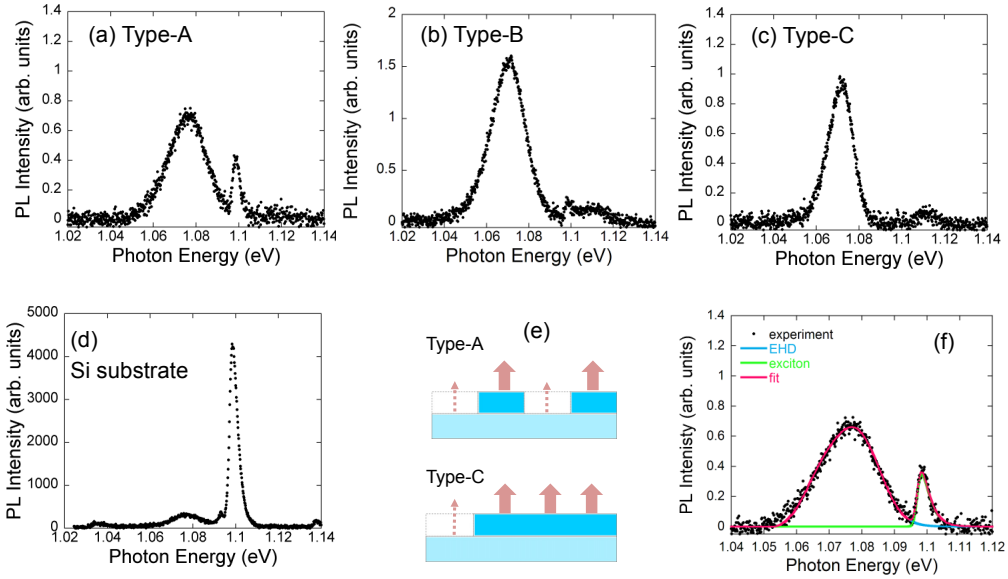

Fig. 3. (a), (b) and (c) PL spectra at 12 K from the samples, Type-A, Type-B and Type-C, respectively. (d) PL spectra from the Si substrate. The incidence laser power was about 280 Wcm^{-2}. (e) Schematic pictures showing PL emission from Si NW (bold arrow) and Si substrate at the gap between Si NWs (thin arrow). (f) Theoretical curve fitting to the measured PL spectra in the Type-A sample.

In Figs. 3(a)–3(c), on the other hand, broad PL bands with full widths at half maximum (FWHM) of 24, 20 and 13 meV were observed at around 1.076, 1.070, and 1.072 eV, respectively. These broad PL bands, observed often in indirect band gap semiconductors at high optical excitation under the low temperature of [18–20], are attributed to formation of either electron-hole droplet (EHD) or electron-hole plasma (EHP) depending on the carrier temperature and density. The line shape of the broad PL band is calculated and compared with the measured spectra by the following convolution products of electron and hole density of states (DOS) [20],

$$I(h\nu) = I_0 \int_0^{h\bar{\nu}} D_e(\varepsilon) D_h(h\bar{\nu} - \varepsilon) f(\varepsilon, E_F^e) f(h\bar{\nu} - \varepsilon, E_F^h) d\varepsilon \quad . \qquad (1)$$

Here, I_0 is a constant, hv is the photon energy, $D_e(\varepsilon)$ and $D_h(\varepsilon)$ are DOS of electron and hole, respectively, $h\bar{\nu} = h\nu - E_g + \hbar\omega$, E_g is the reduced band-gap energy due to the interactions between electrons and holes in the high-density state, $\hbar\omega$ is the emitted phonon energy. Fitting parameters are E_g, the electron hole pair density, n, and carrier temperature T_e. We use DOS in three dimensions for fitting spectra since the thickness and width of the NW are much larger than the effective Bohr radius, 4.9 nm, of the exciton in the bulk Si. As an example of curve fitting, the calculated line shape of the broad PL band is fit well to the measured PL spectra in Type-A, as shown in Fig. 3(f). The carrier density and temperature in our experiment is estimated to be n = 6.9 × 10^{18} cm^{-3} and T_e = 24 K in the Type-A Si NW with a cross section of 50 × 50 nm^2, n = 5.8 × 10^{18} cm^{-3} and T_e = 26 K in the Type-B with a cross section of 50 × 219 nm^2 and n = 3.6 × 10^{18} cm^{-3} and T_e = 17 K in the Type-C with a cross section of 50 × 386 nm^2. The transition between EHD and EHP in the bulk Si occurs around T_e = 25 K [20]. It was previously reported in Si NWs obtained by copper catalyzed chemical vapor deposition with a diameter in the 50-300 nm range that the EHP was present in the Si NW with n = 3.3 × 10^{18} cm^{-3} and T_e = 46 K [21]. This carrier temperature is higher

#202699 - $15.00 USD Received 6 Dec 2013; accepted 24 Dec 2013; published 23 Jan 2014

than the estimated carrier temperatures of our Si NW samples. It is expected that carrier confinement leads to increase in correlation energy and thus, the transition temperature may increase from the bulk value of about 25 K.

4.2 One- and two-dimensional PL-spectra mapping on the Si NW chip

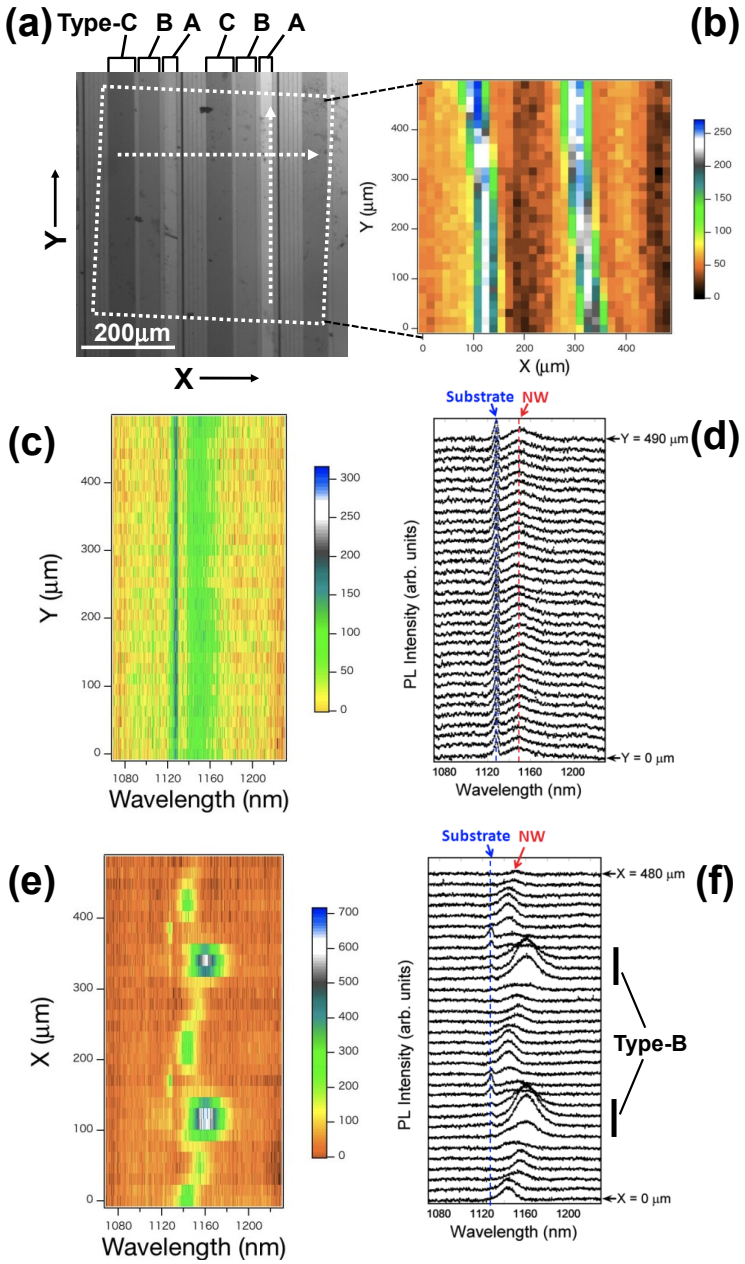

Fig. 4. (a) Optical microscope image of PL-spectra mapping region in the Si NW sample. Square dotted line shows an area of two-dimensional PL-spectra mapping, while vertical and horizontal dotted arrows indicate scanning directions for mapping in (c), (d) and (e), (f), respectively. (b) Mapping of integrated PL intensity between 1140 and 1180 nm at 12 K. (c) Spatially resolved PL intensity and (d) PL spectra scanned along Si NW of the Si width of 50 nm. (e) Spatially resolved PL intensity and (f) PL spectra scanned perpendicular to the wire direction.

#202699 - $15.00 USD Received 6 Dec 2013; accepted 24 Dec 2013; published 23 Jan 2014

For the purpose of investigating the uniformity of the Si NWs, PL spectra mapping was employed by using the Si NWs width the Type-A to Type-C structures, as shown by an SEM plan-view photograph in Fig. 4(a). Here, a white square dotted line shows an area of two-dimensional PL-spectra mapping, while a vertical and horizontal dotted lines show mapping directions for obtaining vertical and horizontal PL-spectra uniformity of the Si NW, respectively.

Figure 4(b) shows the resultant spatial distribution of the integrated PL intensity with the spatial resolution of about 15 μm in the scanned area of 490 × 480 μm^2. Each spectrum wavelength is ranging from 1140 to 1180 nm. In Fig. 4(b), two vertical zones showing the intense PL peaks are observed. This corresponds to the Type-B NW, as shown by the arrows in Fig. 4(b), taking into account that the Type-B NW shows more intense PL than Type-A and Type-C, as shown in Figs. 3(a)–3(c). In addition, these two high-intense PL-zones are a little tilted in Fig. 4(b). This is because the scanned squire area was not just in parallel to the direction of the Si NW, as indicated in Fig. 4(a), and not as a result of non-uniform patterning of the Si NW.

Uniformity of the Si NW is also shown by the following two PL intensity maps. Figures 4(c) and 4(d) show spatially resolved integrated PL intensity map and PL spectra, respectively. Here, the scanning was employed along the vertical arrow in Fig. 4(a) by 32 steps from Y = 0 to Y = 490 μm in the Type-A sample. In Fig. 4(d), broad PL band PL peaks at 1149 nm (1.077 eV) and narrow-band peaks at 1128 nm (1.098 eV) are specific to the Si NW at high optical excitation density and the exciton in the Si substrate, as discussed in Figs. 3(a)–3(c). It should be noted that excellent vertical alignment of both broad PL band and exciton-related PL peak lines indicates that Si NWs are formed with excellent uniformity over a large area. Similarly, Figs. 4(e) and 4(f) show spatially resolved integrated PL intensity map and PL spectra scanned along the horizontal arrow in Fig. 4(a) by 32 steps from X = 0 to X = 480 μm. In Fig. 4(f), each PL spectrum is obtained from either Type-A, -B or -C Si NW group. Among them, the most intense PL spectra are originating from the Type-B NWs. In Fig. 4(f), exciton-related narrow peaks from the Si substrate are also observed at 1128 nm in several spectra. Uniformity of the Si NW structure is also confirmed by these PL intensity maps as shown here.

4.3 Parameter- dependent PL spectra in the Si NW

In this section, parameter-dependent PL spectra in the Si NWs are investigated. Figures 5(a) and 5(b) show Si NW-width dependence of PL peak energies with different annealing temperatures for Type-A and Type-C samples, respectively. For both samples, peak energies are increasing with decrease in Si width. The result reminds us of appearance of a quantum confinement effect in the Si NW. Here, we look into the origin of the peak energy shift more deeply. It is known that the exciton's effective Bohr radius is 4.9 nm in the Si NW, while the thickness (50 nm) as well as the width (24 ~386 nm for the Type-A and -C) of the Si NW used in our experiment are one or two orders of magnitudes larger than the Bohr radius. Accordingly, the quantum confinement effect is likely to be negligible qualitatively. Indeed, according to the effective mass theory and assuming assumption of infinite potential barriers, increase of the energy in changing the state from the bulk state to the quantum-confined state within the thickness d in Si is given by

$$\Delta E = \frac{\pi^2 h^2}{2d^2}\left(\frac{1}{m_e^*} + \frac{1}{m_h^*}\right) \tag{2}$$

where m_e^* and m_h^* are the density-of-state effective mass of electron and hole, respectively [22–24]. One finds $\Delta E \cong 0.4$ meV from Eq. (2) for $d = 50$ nm using $m_e^* = 1.062\, m_0$ and $m_h^* = 0.591\, m_0$ at 4.2 K, resulting in that the value is much smaller than the measured energy shifts, 2 ~8 meV in Figs. 5(a) and 5(b). Eventually the simplified quantum confinement model

#202699 - $15.00 USD Received 6 Dec 2013; accepted 24 Dec 2013; published 23 Jan 2014

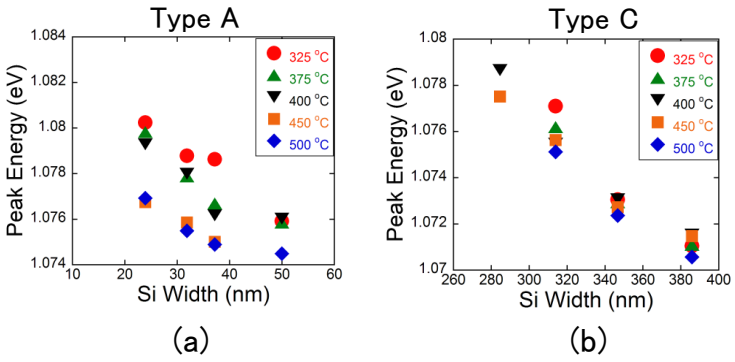

Fig. 5. (a) and (b) show Si NW width dependences of PL peak energies with different annealing temperatures for the samples in Type-A and Type-B, respectively.

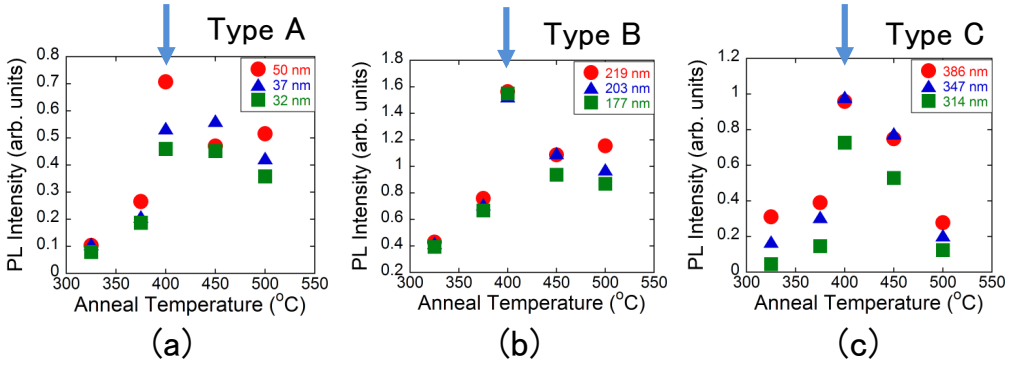

Fig. 6. (a), (b) and (c) show annealing temperature dependences of PL peak intensities with different widths for the samples in Type-A, Type-B and Type-C, respectively.

shown here is likely to be unsuitable for evaluating the origin of the energy shift in Fig. 5. Another possible origin of the peak energy shift is an effect of the strain at the interface between Si and SiO_2. A molar volume mismatch between Si and SiO_2 causes stressed region in both Si and SiO_2. Simulations of a Si NW surrounded by SiO_2 revealed that Si lattice has compressive stress near the interface between Si and SiO_2 [25,26] and, in addition, 1% compressive strain in Si NW lowers the bottom of conduction band by about 0.1 eV [27,28]. The estimated strain-induced decrease in energy (0.1eV) might be comparable to the measured energy shift (~8meV) depending on the strain amplitude. However, it is not consistent with the experimental result that the energy increases with decrease of Si NW width, as shown in Fig. 5. At the moment, single mechanism of either quantum confinement or strain effect mentioned above is not enough for explaining the origin of the peak energy shift in Fig. 5 and it is likely that more complex mechanism available for the NW structure should be needed.

On the other hand, annealing temperature dependence of PL peak intensities of Si NWs in Type-A, Type-B and Type-C are shown in Figs. 6(a)–6(c), respectively. Measurements were employed for the samples with different NW widths, as indicated in insets. It is found that the PL peak intensity is maximized at 400 °C for each NW type. It is reported that annealing in H_2 forming gas introduces hydrogen into near-interfacial oxide region to passivate the dangling Si bonds called P_b centers [29–31]. Moreover, the amount of such H and resultant density change in the interface defects are strongly affected by the annealing temperature. In more detail, reduction of PL intensity at higher temperatures than 400 °C is reported as a result of the H uptake and its desorption from the oxide region [29]. Our results in Fig. 6 are

#202699 - $15.00 USD Received 6 Dec 2013; accepted 24 Dec 2013; published 23 Jan 2014

quite consistent with these previous reports. Therefore, the result means that the technique of micro-PL measurement mentioned above is quite useful as a nondestructive method of characterizing Si nanostructures like NW reported here.

5. Conclusion

Low-temperature PL spectra of electron-hole systems in Si NWs prepared by thermal oxidization of Si fin structures were studied. Quite uniform Si NWs with thickness of 50nm and widths ranging from 24nm to 386nm were successfully fabricated. A broad PL band was observed at a peak energy (1.07 – 1.08 eV) lower than that (1.10 eV) for exciton-related narrow band specific to the Si substrate. Mapping of PL reveals that NWs with uniform width are formed over a large area. As a result of studying a parameter-dependent PL peak energy, blue-shift in the PL peak energy with decrease in the Si NW width was observed in all the samples. Annealing temperature dependence of PL peak intensities also confirmed that the micro-PL demonstrated here is one of the important methods for characterizations of the interface defects in Si NWs.

Acknowledgments

The authors would like to express their sincere appreciation to K. Asakawa and K. Murakami for advice throughout this research. This work was partly supported by Kakenhi Nos. 20104005, 25103704, and NEDO's Innovation Research Project on Nanoelectronics Materials and Structures.

#202699 - $15.00 USD Received 6 Dec 2013; accepted 24 Dec 2013; published 23 Jan 2014